arXiv:1304.4195v2 [cond-mat.mtrl-sci] 17 Apr 2013

Field dependence of the Spin State and Spectroscopic Modes of Multiferroic BiFeO$_3$

Randy S. Fishman
Materials Science and Technology Division, Oak Ridge National Laboratory, Oak Ridge, Tennessee 37831, USA
(Dated: April 18, 2013)

The spectroscopic modes of BiFeO$_3$ provide detailed information about the very small anisotropy and Dzyaloshinskii-Moriya (DM) interactions responsible for the long-wavelength, distorted cycloid that appears below $T_{\rm N} = 640$ K. A microscopic model that includes two DM interactions and easy-axis anisotropy is able to closely describe both the zero-field spectroscopic modes as well as their splitting and evolution in a magnetic field. While only six modes are optically active in zero field, all of the zone-center modes are activated by a magnetic field. The close agreement with experiment suggests that the proposed model provides the foundation for future technological applications of this multiferroic material.

PACS numbers: 75.25.-j, 75.30.Ds, 78.30.-j, 75.50.Ee

Due to the coupling between electric and magnetic properties, mutliferroic materials are among the most important yet discovered. With a multiferroic material used as a storage medium, information can be written electrically and then read magnetically without Joule heating[1]. Hence, applications of a room-temperature multiferroic would radically transform the magnetic storage industry. Because it is the only known room-temperature multiferroic, BiFeO$_3$ continues to attract intense interest.

Although its ferroelectric transition temperature[2] $T_c \approx 1100$ K is much higher than its Néel transition temperature[3–5] $T_{\rm N} \approx 640$ K, the appearance of a long-wavelength cycloid[3,6–8] with a period of 62 nm enhances the ferroelectric polarization below $T_{\rm N}$. The induced polarization has been used to switch between magnetic domains with an applied electric field[4,5,9].

Progress in understanding the microscopic interactions in BiFeO$_3$ has been greatly accelerated by the recent availability of single crystals for both elastic and inelastic neutron-scattering measurements. By fitting the spin-wave (SW) frequencies above a few meV, recent inelastic measurements[10,11] have determined the antiferromagnetic (AF) nearest-neighbor and next-nearest neighbor exchanges $J_1 \approx -4.5$ meV and $J_2 = -0.2$ meV, indicated in the pseudo-cubic unit cell of Fig.1(a) with lattice constant $a \approx 3.96\,\mathring{A}$. In the presence of strain[12,13] or a magnetic field[14,15] above $H_c \approx 20$ T, those exchange interactions produce a G-type AF with ferromagnetic (FM) alignment of the $S = 5/2$ Fe^{3+} spins within each hexagonal plane.

The cycloidal magnetic order in BiFeO$_3$ below H_c is produced by the much smaller anisotropy and Dzyaloshinskii-Moriya (DM) interactions. Because the wavelength $a/\sqrt{2}\delta$ of BiFeO$_3$ is so large, inelastic neutron-scattering measurements do not have the $\mathbf{q}$-space resolution needed to resolve the cycloidal satellites at $\mathbf{q} = (2\pi/a)(0.5 \pm \delta, 0.5, 0.5 \mp \delta)$, on either side of the AF wavevector $\mathbf{Q}_0 = (\pi/a)(1,1,1)$. Below 5 meV, inelastic measurements at $\mathbf{Q}_0$ reveal four broad peaks, each of which can be roughly assigned to one or more of the SW branches averaged over the first Brillouin zone[11,16].

By contrast, THz spectroscopy[17,18] provides very precise measurements for the optically-active SW modes at the cycloidal wavevector $\mathbf{Q}$. For polarization along $\mathbf{z}' = [1,1,1]$ (all unit vectors are assumed normalized to 1), the three magnetic domains have ordering wavevectors $\mathbf{Q}_1 = (2\pi/a)(0.5+\delta, 0.5-\delta, 0.5)$ (domain 1), $\mathbf{Q}_2 = (2\pi/a)(0.5+\delta, 0.5, 0.5-\delta)$ (domain 2), and $\mathbf{Q}_3 = (2\pi/a)(0.5, 0.5+\delta, 0.5-\delta)$ (domain 3). The local coordinate system $\{x', y', z'\}$ for each domain is indicated in Fig.1.

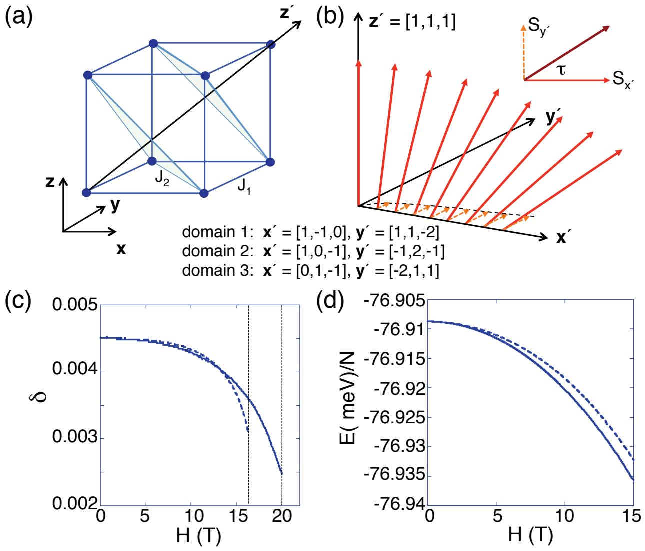

FIG. 1: (a) The pseudo-cubic cell with exchange interactions J_1 and J_2 as well as the polarization direction $\mathbf{z}'$ cutting through two hexagonal planes. (b) For any of the three magnetic domains, a schematic of the spins in zero field showing their rotation about $\mathbf{y}'$. Due to the DM interaction $\mathbf{D}' = D'\mathbf{z}'$, spins rotate by τ about $\mathbf{z}'$ in the $x'y'$ plane. (c) The wavevector parameter δ versus field for domain 1 (solid) and domains 2 and 3 (dashed) with vertical dashed lines showing their critical fields. (d) The energies of domains 1 (solid) and domains 2 and 3 (dashed) versus field. Both (c) and (d) assume that the field is along [0,0,1].

In zero field, the four observed mode frequencies were recently described by a model[19] with two DM interactions and easy-axis anisotropy K along $\mathbf{z}'$. While the DM interaction D along $\mathbf{y}'$ is responsible for the cycloidal period, the DM interaction[20–23] D' along $\mathbf{z}'$ produces a small tilt[22] τ in the cyloidal plane, shown in Fig.1(b), which alternates in sign from one hexagonal plane to the next. In the canted AF phase above H_c, D' produces a weak FM moment[14,15] of about $\mathbf{M}_0 = 0.03\mu_{\rm B}\mathbf{y}'$.

This Letter shows that the microscopic model described above also predicts the mode splitting and evolution of the spectroscopic modes with field. Due to mode mixing, all of the SWs are optically active in a magnetic field. The mode splitting and field dependence allows us to unambiguously assign the spectroscopic modes of BiFeO$_3$. The close agreement between predictions and measurements suggests that the proposed model can provide the foundation for future work on BiFeO$_3$.

In a magnetic field $\mathbf{H} = H\mathbf{m}$ along $\mathbf{m}$, the spin state and SW excitations of BiFeO$_3$ are evaluated from the Hamiltonian

$$\begin{aligned}\mathcal{H} = &-J_1\sum_{\langle i,j\rangle}\mathbf{S}_i\cdot\mathbf{S}_j - J_2\sum_{\langle i,j\rangle'}\mathbf{S}_i\cdot\mathbf{S}_j - K\sum_i(\mathbf{S}_i\cdot\mathbf{z}')^2\\ &-D\sum\nolimits_{\mathbf{R}_j=\mathbf{R}_i+a(\mathbf{x}-\mathbf{z})}\mathbf{y}'\cdot(\mathbf{S}_i\times\mathbf{S}_j)\\ &-D'\sum\nolimits_{\mathbf{R}_j=\mathbf{R}_i+a\mathbf{x},a\mathbf{y},a\mathbf{z}}(-1)^{R_{iz'}/c}\,\mathbf{z}'\cdot(\mathbf{S}_i\times\mathbf{S}_j)\\ &-2\mu_{\rm B}H\sum_i\mathbf{S}_i\cdot\mathbf{m}. \end{aligned}\tag{1}$$

While the nearest- and next-nearest neighbor exchange interactions $J_1 = -4.5$ meV and $J_2 = -0.2$ meV can be obtained from the SW dispersion between 5.5 meV and 72 meV[10,11], the small interactions D, D', and K that control the cycloid can be obtained from THz spectroscopy below 5.5 meV (44.3 cm^{-1}).

For a given set of interaction parameters and magnetic field, the spin state of BiFeO$_3$ is obtained by minimizing the energy $E = \langle\mathcal{H}\rangle$ over a set of variational parameters. With the same spin states in hexagonal layers n and $n+2$, we parameterize the spin states in layers $n = 1$ and 2 as

$$\begin{aligned} S_{x'}(\mathbf{R}) &= A^{(n)}(\mathbf{R})\sin\mu\,\cos\tau^{(n)}\,\sin(2\pi\delta R_{x'}/a+\gamma_1^{(n)})\\ &+\ s_0p_{x'}^{(n)}, &(2)\\ S_{y'}(\mathbf{R}) &= A^{(n)}(\mathbf{R})\sin\mu\,\sin\tau^{(n)}\,\sin(2\pi\delta R_{x'}/a+\gamma_2^{(n)})\\ &+\ s_0p_{y'}^{(n)}, &(3)\\ S_{z'}(\mathbf{R}) &= A^{(n)}(\mathbf{R})\cos\mu\,F^{(n)}(\mathbf{R})+s_0p_{z'}^{(n)}, &(4)\end{aligned}$$

where

$$\begin{aligned}F^{(n)}(\mathbf{R}) = &\sum_{l=1}C_{2l-1}\cos\bigl(2(2l-1)\pi\delta R_{x'}/a\bigr)\\ &+\sum_{l=1}C_{2l}\cos\bigl(4l\pi\delta R_{x'}/a+\Gamma^{(n)}\bigr)\end{aligned}\tag{5}$$

and we take $C_1 = 1$. Notice that the unit vectors $\mathbf{p}^{(n)}$ and the tilt angles $\tau^{(n)}$ can be different for layers 1 and 2. Four phases $\gamma_1^{(n)}$ and $\gamma_2^{(n)}$ parameterize $S_{x'}(\mathbf{R})$ and $S_{y'}(\mathbf{R})$. In zero field, the higher odd harmonics $C_{2l+1>1}$ in $F^{(n)}(R_{x'})$ are produced by either the anisotropy K or the DM interaction D'. In addition, even harmonics C_{2l} are produced by the magnetic field. Because the coefficients C_l fall off rapidly with l, we neglect harmonics above $l = 4$. The additional variable $\Gamma^{(n)}$ on each layer allows the even and odd harmonics to be out of phase. On layer n and site $\mathbf{R}$, the amplitude $A^{(n)}(\mathbf{R})$ is fixed by the condition that $|\mathbf{S}(\mathbf{R})| = S$, which is satisfied by a quadratic equation for $A^{(n)}(\mathbf{R})$. The lower root is used for layer 1; the upper root is used for layer 2.

Fixing $\delta = 1/q$, where $q \gg 1$ is an integer, E is minimized over the 17 variational parameters (μ, $\tau^{(n)}$, $\gamma_i^{(n)}$, $\Gamma^{(n)}$, $\mathbf{p}^{(n)}$, $C_{l\le 4}$, and s_0) on a unit cell with q sites along $\mathbf{x}'$ and two hexagonal layers. Another minimization loop is then performed over q to determine the cycloidal wavevector as a function of field. In zero field, $q = 222$. We verify that the corresponding spin state provides at least a metastable minimum of the energy by checking that the classical forces on each spin vanish. Another check is that the SW frequencies calculated below are all real.

We emphasize that the variational parameters are not free but rather are functions of the interaction parameters D, D', and K, and the magnetic field H. In zero field, the spin state reduces to the one used in Ref.[19]. A much simpler variational form for the spin state would have been possible were the field oriented along the high-symmetry axis $\mathbf{z}' = [1, 1, 1]$. The complex form given by Eqs.(2-4) is required because the experimental field is oriented along $[0, 0, 1]$. Above H_c, the canted phase with $\delta = 0$ can be more simply parameterized by taking $C_{l>1} = 0$, $\tau^{(1)} = \tau^{(2)}$, $\Gamma^{(n)} = 0$, and $\mathbf{p}^{(n)} = \mathbf{m}$, thereby reducing the number of variational parameters to 7.

Taking $\mathbf{m} = [0, 0, 1]$, $|\mathbf{m}\cdot\mathbf{x}'|$ and $|\mathbf{m}\cdot\mathbf{y}'|$ are the same for domains 2 and 3. Therefore, their equilibrium and dynamical properties are identical. In Fig.1(c), we plot δ versus field for the three domains. Notice that the critical field $H_c = 16.4$ T for domains 2 and 3 is lower than $H_c = 20.2$ T for domain 1. The variation of H_c with $\mathbf{m}$ was recently reported in Ref.[15] and was predicted by Le Bras *et al.*[24] for a purely harmonic cycloid. In zero field, all three domains have the same energy. But in a nonzero field, domain 1 has lower energy than domains 2 and 3, as seen in Fig.1(d). At 5 T, the energy difference between domains is about 0.9 μeV/site.

Generally, the spin-spin correlation function $S_{\alpha\beta}(\mathbf{q},\omega)$ may be expanded in a series of delta functions at each SW frequency $\omega_m(\mathbf{q})$:

$$S_{\alpha\beta}(\mathbf{q},\omega) = \sum_m \delta\bigl(\omega-\omega_m(\mathbf{q})\bigr)S_{\alpha\beta}^{(m)}(\mathbf{q}),\tag{6}$$

which assumes that the SWs are not damped. The mode frequencies $\omega_m(\mathbf{q})$ and the corresponding intensities $S_{\alpha\beta}^{(m)}$ are solved by using the $1/S$ formalism outlined in Ref.[25] and in Appendix A of Ref.[19] for non-collinear spins. With $\delta = 1/q$, the unit cell contains $2q$ sublattices.

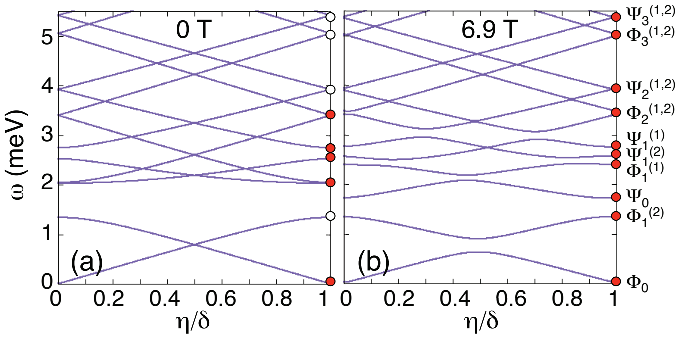

FIG. 2: The mode frequencies versus $\mathbf{q}$ for (a) 0 T and (b) 6.9 T in domain 1. Optically-active modes at $\eta = \delta$ are denoted by filled circles, inactive ones by white circles.

Only some of the SW modes are optically active with non-zero magnetic resonance (MR) matrix elements $|\langle\delta|M_\alpha|0\rangle|$, where $M_\alpha = 2\mu_B \sum_i S_{i\alpha}$ is the magnetization operator, $|0\rangle$ is the ground state with no SWs, and $|\delta\rangle$ is an excited state with a single SW mode at the cycloidal wavevector. A subset of the MR modes are also electromagnetically (EM) active with nonzero matrix elements $|\langle\delta|P_\alpha^{\rm ind}|0\rangle|$, where $\mathbf{P}^{\rm ind}$ is the operator for the electric polarization induced by the cycloid. Expressions for $|\langle\delta|M_\alpha|0\rangle|$ and $|\langle\delta|P_\alpha^{\rm ind}|0\rangle|$ are provided in Appendix B of Ref.[19].

For zero field with $\delta = 1/222$, we adjusted[19] the interaction parameters of BiFeO$_3$ to fit the observed spectroscopic modes[17] at 17.5, 20.1, 21.5, and 27.3 cm^{-1}. Using the weak FM moment $M_0 = 0.03\mu_B$ above H_c to fix[26] $D' = M_0 J_1/\mu_B S$, we obtained the interaction parameters $D = 0.107$ meV, $D' = 0.054$ meV, and $K = 0.0035$ meV. We now employ those interaction parameters to describe the field dependence of the spectroscopic modes in BiFeO$_3$.

In Fig.2, we plot the SW frequencies versus $\mathbf{q} = (2\pi/a)(0.5+\eta, 0.5-\eta, 0.5)$ for domain 1 and $H = 0$ or 6.9 T. To label the spectroscopic modes at $\mathbf{q} = \mathbf{Q}$ or $\eta = \delta$, we have modified the notation of de Sousa and Moore[27], who studied the case where D' and K vanish and the cycloid is purely harmonic. In an extended zone scheme, they labeled the SW modes at wavevector nQ as Ψ_n and Φ_n. Corresponding to excitations within the cycloidal plane, $\Phi_n = \Phi_1|n|$ is a linear function of n. The out-of-plane modes satisfy the relation $\Psi_n = \Phi_1\sqrt{1+n^2}$. Due to the higher harmonics of the cycloid[16,19] produced by D' or K, $\Psi_{n>0}$ and $\Phi_{n>0}$ each split into two modes that we label as $\Psi_{n>0}^{(1,2)}$ and $\Phi_{n>0}^{(1,2)}$.

Only Φ_0, Ψ_0, $\Phi_1^{(1)}$, $\Psi_1^{(2)}$, $\Psi_1^{(1)}$, and $\Phi_2^{(1)}$ are optically active in zero field. Those six modes are indicated by the filled circles in Fig.2(a). Although the lowest-frequency Φ_0 mode has an enormous SW intensity and MR matrix element $|\langle\delta|M_{y'}|0\rangle|$, it is not detectable by THz measurements. At 21.5 cm^{-1}, $\Psi_1^{(1)}$ with $|\langle\delta|M_{x'}|0\rangle| > 0$ is also EM active. The nearly-degenerate Ψ_0 and $\Phi_1^{(1)}$ modes with significant $|\langle\delta|M_{x'}|0\rangle|$ and $|\langle\delta|M_{y'}|0\rangle|$ matrix elements, respectively, are responsible for the observed spectroscopic peak[17] at 17.5 cm^{-1}. While $\Psi_1^{(2)}$ is activated by the 3$\mathbf{Q}$ harmonic of the cycloid, which mixes $\Psi_1^{(2)}$ with $\Psi_1^{(1)}$, Ψ_0 and $\Phi_1^{(1)}$ are activated by the tilt of the cycloid out of the $x'z'$ plane, which mixes Ψ_0 with $\Psi_1^{(1)}$ and $\Phi_1^{(1)}$ with Φ_0.

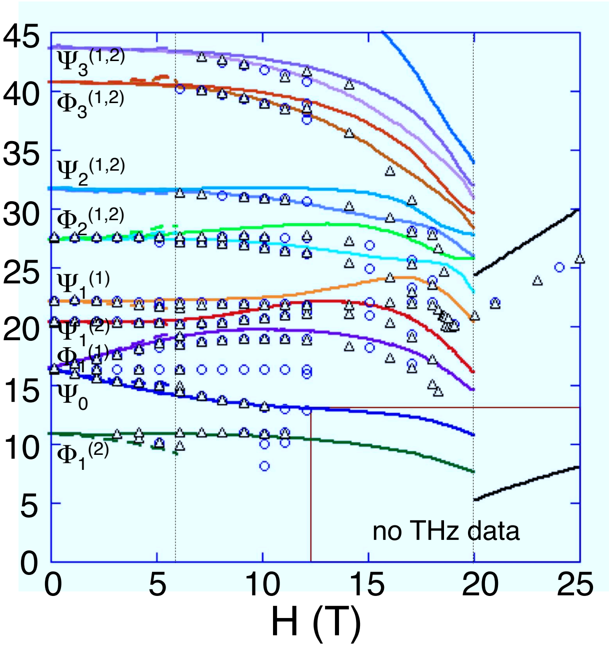

FIG. 3: The measured spectroscopic frequencies with *rf* field $\mathbf{h}_1$ (circles) or $\mathbf{h}_2$ (triangles). The predicted mode frequencies from domain 1 (solid) and domains 2 and 3 (dashed) are also shown. We conjecture that contributions from domains 2 and 3 stop at 6 T, indicated by a dashed vertical line.

In nonzero field, all of the zone-center SW modes are optically active with nonzero MR matrix elements. Many of these modes also have nonzero EM matrix elements. The MR-active modes below 5.5 meV are indicated in Fig.2(b). Notice that Ψ_0 and $\Phi_1^{(1)}$ are split by the magnetic field.

With $\mathbf{m} = [0,0,1]$, the measured field-dependence[18,28] of the spectroscopic modes is plotted in Fig.3. The frequency-dependent magnetic field was aligned either along $\mathbf{h}_1 = [1,-1,0]$ (circles) or $\mathbf{h}_2 = [1,1,0]$ (triangles). These *rf* fields couple to the MR matrix elements $|\langle\delta|\mathbf{M}\cdot\mathbf{h}_m|0\rangle|$. The observed transition to the canted phase occurs just below 20 T. Due to instrumental lim-

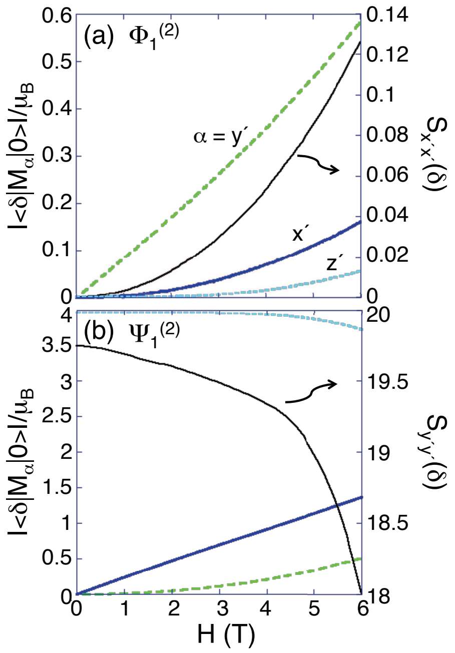

FIG. 4: The evolution of the matrix elements $|\langle\delta|M_\alpha|0\rangle|/\mu_B$ with field for (a) $\Phi_1^{(2)}$ and (b) $\Psi_1^{(2)}$ in domain 1, where $\alpha = x'$ (solid), y' (medium dash), or z' (small dash). On the right are the intensities $S_{x'x'}(\delta)$ and $S_{y'y'}(\delta)$ (thin solid curves) of those modes.

itations, no THz data is available for fields above 12 T and frequencies below about 12 cm^{-1}.

This figure also contains the predicted spectroscopic frequencies for domain 1 (solid), and domains 2 and 3 (dashed). We believe that the energy difference between domains is responsible for depopulating domains 2 and 3 above about 6 T, indicated by a dashed vertical line. To reflect this behavior, we have cut off the predicted mode frequencies of domains 2 and 3 above 6 T.

The agreement between the measured and predicted mode frequencies in Fig.3 is remarkable. In agreement with predictions, Ψ_0 and $\Phi_1^{(1)}$ are slightly lower in domain 1 than in domains 2 and 3. The predicted splitting of $\Phi_2^{(1,2)}$ is clearly seen in Fig.3. Also in agreement with predictions, $\Psi_1^{(1)}$ is slightly lower in domains 2 and 3 than in domain 1. The only feature that remains unexplained by our model is the field-independent mode observed at about 16.5 cm^{-1} midway between $\Phi_1^{(1)}$ and Ψ_0. Notice that spectroscopic modes never cross with field due to their coupling. Because the constant 16.5 cm^{-1} mode appears to be immune to mode repulsion, we speculate that it may be an optical phonon.

The curves in Figs.3 include several modes that become optically active only in a magnetic field H. At 10.8 cm^{-1}, $\Phi_1^{(2)}$ has no active MR matrix elements in zero field but develops significant matrix elements $|\langle\delta|M_{x'}|0\rangle|$ and $|\langle\delta|M_{y'}|0\rangle|$ in a field, as shown in Fig.4(a). The SW intensity $S_{x'x'}(\delta)$ of $\Phi_1^{(2)}$ grows like H^2. Experimentally, $\Phi_1^{(2)}$ appears above about 3 T.

The selection rules governing the observation of the spectroscopic modes also change with external magnetic field H. At 20.4 cm^{-1}, $\Psi_1^{(2)}$ has $|\langle\delta|M_{z'}|0\rangle| > 0$ at zero field. Since $\mathbf{h}_1 \cdot \mathbf{z}' = 0$ but $\mathbf{h}_2 \cdot \mathbf{z}' \neq 0$, $\Psi_1^{(2)}$ is only observable in *rf* field $\mathbf{h}_2$, given by the triangles in Fig.3. But Fig.4(b) shows that $|\langle\delta|M_{x'}|0\rangle|$ increases linearly with field, which explains why $\Psi_1^{(2)}$ appears in *rf* field $\mathbf{h}_1$ when $H > 0$. The intensity $S_{y'y'}(\delta)$ of $\Psi_1^{(2)}$ decreases only slightly with H up to 6 T.

Recall that we use the same interaction parameters previously obtained for zero field[19]. Therefore, it is not surprising that the quantitative agreement with measurements, although quite good, is not perfect. In particular, the measured spectroscopic frequency of the canted phase above H_c is about 4 cm^{-1} lower than predicted. Improvements might be acheived by using slightly higher values[26] of D'.

To conclude, the close agreement between the predicted and observed spectroscopic frequencies with field leaves no doubt about the origin of those modes. This agreement suggests that the present model, with DM interactions along $\mathbf{y}'$ and $\mathbf{z}'$ and easy-axis anisotropy along $\mathbf{z}'$, can provide the foundation for future studies on BiFeO$_3$ and may lay the groundwork for its eventual technological applications.

I gratefully acknowledge conversations with Nobuo Furukawa, Masaaki Matsuda, Shin Miyahara, Satoshi Okamoto, Urmas Nagel, Toomas Rõõm, and Rogero de Sousa. Research sponsored by the U.S. Department of Energy, Office of Basic Energy Sciences, Materials Sciences and Engineering Division.

---

[1] W. Eerenstein, N.D. Mathur, and J.F. Scott, Nat. **442**, 759 (2006).
[2] J.R. Teague, R. Gerson, and W.J. James, Solid State Commun. **8**, 1073 (1970).
[3] I. Sosnowska, T. Peterlin-Neumaier, and E. Steichele, J. Phys. C: Solid State Phys. **15**, 4835 (1982).
[4] D. Lebeugle, D. Colson, A. Forget, M. Viret, A.M. Bataille, and A. Gukasov, Phys. Rev. Lett. **100**, 227602 (2008).
[5] S. Lee, W.M. Ratcliff II, S.-W. Cheong, and V. Kiryukhin, Appl. Phys. Lett. **92**, 192906 (2008).
[6] M. Ramazanoglu, W. Ratcliff II, Y.J. Choi, S. Lee, S.-W. Cheong, and V. Kiryukhin, Phys. Rev. B **83**, 174434 (2011).
[7] J. Herrero-Albillos, G. Catalan, J.A. Rodriguez-Velamazan, M. Viret, D. Colson, and J.F. Scott, J. Phys.: Condens. Matter **22**, 256001 (2010).
[8] I. Sosnowska and R. Przenioslo, Phys. Rev. B **84**, 144404 (2011).

[9] S. Lee. T. Choi, W. Ratcliff II, R. Erwin, S.-W. Cheong, and V. Kiryukhin, Phys. Rev. B **78**, 100101(R) (2008).

[10] J. Jeong, E.A. Goremychkin, T. Guidi, K. Nakajima, G.S. Jeon, S.-A. Kim, S. Furukawa, Y.B. Kim, S. Lee, V. Kiryukhin, S.-W. Cheong, and J.-G. Park, Phys. Rev. Lett. **108**, 077202 (2012).

[11] M. Matsuda, R.S. Fishman, T. Hong, C.H. Lee, T. Ushiyama, Y. Yanagisawa, Y. Tomioka, and T. Ito, Phys. Rev. Lett. **109**, 067205 (2012).

[12] F. Bai, J. Wang, M. Wuttig, J.F. Li, N. Wang, A.P. Pyatakov, A.K.Zvezdin, L.E. Cross, and D. Viehland, Appl. Phys. Lett. **86**, 032511 (2005).

[13] P. Chen, Ö. Günaydın-Sen, W.J. Ren, Z. Qin, T.V. Brinzari, S. McGill, S.-W. Cheong, and J.L. Musfeldt, Phys. Rev. B **86**, 014407 (2012).

[14] M. Tokunaga, M. Azuma, and Y. Shimakawa, J. Phys. Soc. Jpn. **79**, 064713 (2010).

[15] J. Park, S.-H. Lee, S. Lee, F. Gozzo, H. Kimura, Y. Noda, Y.J. Choi, V. Kiryukhin, S.-W. Cheong, Y. Jo, E.S. Choi, L. Balicas, G.S. Jeon, and J.-G. Park, J. Phys. Soc. Jpn. **80**, 114714 (2011).

[16] R.S. Fishman, N. Furukawa, J.T. Haraldsen, M. Matsuda, and S. Miyahara, Phys. Rev. B **86**, 220402 (R) (2012).

[17] D. Talbayev, S.A. Trugman, S. Lee, H.T. Yi, S.-W. Cheong, and A.J. Taylor, Phys. Rev. B **83**, 094403 (2011).

[18] U. Nagel, T. Katuwal, H. Engelkamp, D. Talbayev, H.T. Yi, S.-W. Cheong, and T. Rõõm, cond.-mat.:1302.2491.

[19] R.S. Fishman, J.T. Haraldsen, N. Furukawa, and S. Miyahara, Phys. Rev. B (*in press*).

[20] A.M. Kadomtseva, A.K. Zvezdin, Yu.F. Popv, A.P. Pyatakov, and G.P. Vorob'ev, JTEP Lett. **79**, 571 (2004).

[21] C. Ederer and N.A. Spaldin, Phys. Rev. B **71**, 060401(R) (2005).

[22] A.P. Pyatakov and A.K. Zvezdin, Eur. Phys. J. B **71**, 419 (2009).

[23] K. Ohoyama, S. Lee, S. Yoshii, Y. Narumi, T. Morioka, H. Nojiri, G.S. Jeon, S.-W. Cheong, and J.-G. Park, J. Phys. Soc. Jpn. **80**, 125001 (2011).

[24] G. Le Bras, D. Colson, A. Forget, N. Genand-Riondet, R. Tourbot, and P. Bonville, *Phys. Rev. B* **80**, 134417 (2009).

[25] J.T. Haraldsen and R.S. Fishman, J. Phys.: Condens. Matter **21**, 216001 (2009).

[26] The estimate $\mathbf{M}_0 = 0.03\mu_\mathrm{B}\mathbf{y}'$ is based on an analysis of the magnetization curves[14,15] assuming that $\mathbf{m} = \mathbf{y}'$. If the field is oriented away from $\mathbf{y}'$, then the extrapolated zero-field FM moment would be less than M_0 and a slightly larger value of D' would be obtained.

[27] R. de Sousa and J.E. Moore, Phys. Rev. B **77**, 012406 (2008).

[28] The data plotted in Fig.3 does not include the observed $H = 0$ modes[18] at 18.1 and 18.2 cm^{-1} because they only appear in zero field.